Developmental Biology 350 (2011) 267–278

Contents lists available at ScienceDirect

Developmental Biology

journal homepage: www.elsevier.com/developmentalbiology

PAT-12, a potential anti-nematode target, is a new spectraplakin partner essential for *Caenorhabditis elegans* hemidesmosome integrity and embryonic morphogenesis

Suzannah Hetherington [a,b,1], Christelle Gally [b,1], Julie-Anne Fritz [a], Jolanta Polanowska [c,d,e], Jérôme Reboul [c,d,e], Yannick Schwab [f], Hala Zahreddine [b], Carolyn Behm [a,*], Michel Labouesse [b,*]

[a] Research School of Biology, College of Medicine, Biology and Environment, Tthe Australian National University, Canberra ACT 0200, Australia
[b] Development and Stem Cells Program, IGBMC, CNRS UMR7104, INSERM U964, Université de Strasbourg BP. 10142, 1, rue Laurent Fries, 67404 Illkirch Cedex, France
[c] INSERM, U891, Centre de Recherches en Cancérologie de Marseille, Marseille, F-13009,France
[d] Institut Paoli-Calmettes, Marseille, F-13009, France
[e] Univ Méditerranée, F-13007, Marseille, France
[f] Imaging Center, IGBMC, CNRS UMR7104, INSERM U964, Université de Strasbourg BP. 10142, 1, rue Laurent Fries, 67404 Illkirch Cedex, France

ARTICLE INFO

Article history:
Received for publication 18 October 2010
Revised 19 November 2010
Accepted 23 November 2010
Available online 3 December 2010

Keywords:
Parasitic nematode
Fibrous organelle
Hemidesmosome
Epithelial
Morphogenesis
Cytoskeleton
Plakin
Cell-matrix attachment
B20 antigen

ABSTRACT

Caenorhabditis elegans embryonic elongation depends on both epidermal and muscle cells. The hemidesmosome-like junctions, commonly called fibrous organelles (FOs), that attach the epidermis to the extracellular matrix ensure muscle anchoring to the cuticular exoskeleton and play an essential role during elongation.
To further define how hemidesmosomes might control elongation, we searched for factors interacting with the core hemidesmosome component, the spectraplakin homolog VAB-10. Using the VAB-10 plakin domain as bait in a yeast two-hybrid screen, we identified the novel protein T17H7.4. We also identified T17H7.4 in an independent bioinformatic search for essential nematode-specific proteins that could define novel anti-nematode drug or vaccine targets. Interestingly, T17H7.4 corresponds to the *C. elegans* equivalent of the parasitic OvB20 antigen, and has a characteristic hemidesmosome distribution. We identified two mutations in *T17H7.4*, one of which defines the uncharacterized gene *pat-12*, previously identified in screens for genes required for muscle assembly. Using isoform-specific GFP constructs, we showed that one *pat-12* isoform with a hemidesmosome distribution can rescue a *pat-12* null allele. We further found that lack of *pat-12* affects hemidesmosome integrity, with marked defects at the apical membrane. PAT-12 defines a novel component of *C. elegans* hemidesmosomes, which is required for maintaining their integrity. We suggest that PAT-12 helps maintaining VAB-10 attachment with matrix receptors.

Introduction

The elongation of tissues plays a critical role in the morphogenesis and organogenesis of many species (Keller, 2006). It generally involves a combination of junction and cytoskeleton remodelling to drive cell shape changes, and can additionally require directed cell division, cell growth, or external forces to favour extension in a certain direction (Butler et al., 2009; Lecuit and Le Goff, 2007). Embryonic morphogenesis has been mainly examined in tissues involving a single cell type (i.e., *Drosophila* germband or trachea, vertebrate notochord). However it can also involve multiple tissues that must then interact with each other. The mechanisms that control such cell–cell interactions during morphogenesis remain poorly understood.

Caenorhabditis elegans provides an elegant model to study this issue. During *C. elegans* embryonic morphogenesis, the embryo elongates four-fold along the anterior-posterior axis in the absence of cell division or cell migration (Priess and Hirsh, 1986). This elongation process depends on three epidermal cell groups (dorsal, ventral and seam) (Chisholm and Hardin, 2005), as well as on muscle cells, which are in contact with the dorsal and ventral epidermal cells, but not with the seam cells (Chisholm and Hardin, 2005; Williams and Waterston, 1994). Embryonic elongation requires intact adherens junctions between epithelial cells, and fibrous organelles (FOs). The latter structure has two roles; it acts like a trans-epithelial tendon, transmitting the force of movement from the muscles to the exoskeleton, and it strengthens the epidermis, rendering it resistant to shearing stress (Zhang and Labouesse, 2010). The contribution of FOs to morphogenesis, and their interplay with cellular processes driving cell shape changes, remain a poorly understood aspect of *C. elegans* morphogenesis.

FOs consist of two hemidesmosome-like junctions connected by cytoplasmic intermediate filaments (cIFs), which mediate epidermal

* Corresponding authors.
E-mail addresses: Carolyn.Behm@anu.edu.au (C. Behm), lmichel@igbmc.fr (M. Labouesse).
[1] These authors contributed equally to this work.

0012-1606/$ – see front matter © 2010 Elsevier Inc. All rights reserved.
doi:10.1016/j.ydbio.2010.11.025

attachment to the cuticle and the basement membrane separating the epidermis from muscles (Fig. 1A) (Francis and Waterston, 1991). The *C. elegans* hemidesmosome-like junctions (abbreviated below CeHD) are structurally, molecularly and functionally related to vertebrate hemidesmosomes (Zhang and Labouesse, 2010). They include, as in vertebrates, a Plectin/BPAG1e homologue (VAB-10A), and cIFs (IFB-1, MUA-6 and IFA-3) (Fig. 1A) (Bosher et al., 2003; Hapiak et al., 2003; Woo et al., 2004). They differ, however, in the transmembrane receptors linking plakin to the extracellular matrix (see Fig. 1A). Absence of most FO proteins leads to FO partial disassembly, and to a loss of epidermal integrity, such that the epidermis expands along the apico-basal axis or detaches from the cuticle and muscles (Bosher et al., 2003; Ding et al., 2003, 2008; Hapiak et al., 2003; Hresko et al., 1999; Woo et al., 2004). Embryos with defective FOs do not elongate beyond the two-fold stage and contain muscles that collapse centrally within the epidermis. The molecular basis for abnormal elongation in CeHD mutants might extend beyond the epidermal integrity problem. Indeed, their actin cytoskeleton, which is essential for elongation, displays some anchoring and bundling defects (Bosher et al., 2003; Ding et al., 2003). Moreover, a recent analysis suggested that hemidesmosome remodelling is coupled to actin remodelling (Zahreddine et al., 2010). Although these data indicate that CeHDs and the actin remodelling machinery might be interdependent, the nature of this link has not yet been defined.

A deeper understanding of the control of elongation by hemidesmosomes requires knowledge of all the components of CeHDs. Here we report the characterization of *pat-12*, which we identified as a novel CeHD component using two parallel and independent strategies. Specifically, one of us (C.B.) was interested in defining genes that could define novel anti-nematode drug or vaccine targets. In the process of screening for such genes, we became interested in a gene that was later identified as *pat-12*. The other group (M.L.) identified the same gene in a yeast two-hybrid screen using as bait the core CeHD component VAB-10A. We describe the expression pattern of the many different *pat-12* isoforms and show that one of them is located in epidermal CeHD. Lack of this isoform specifically affects intermediate filament organization and apical membrane organization.

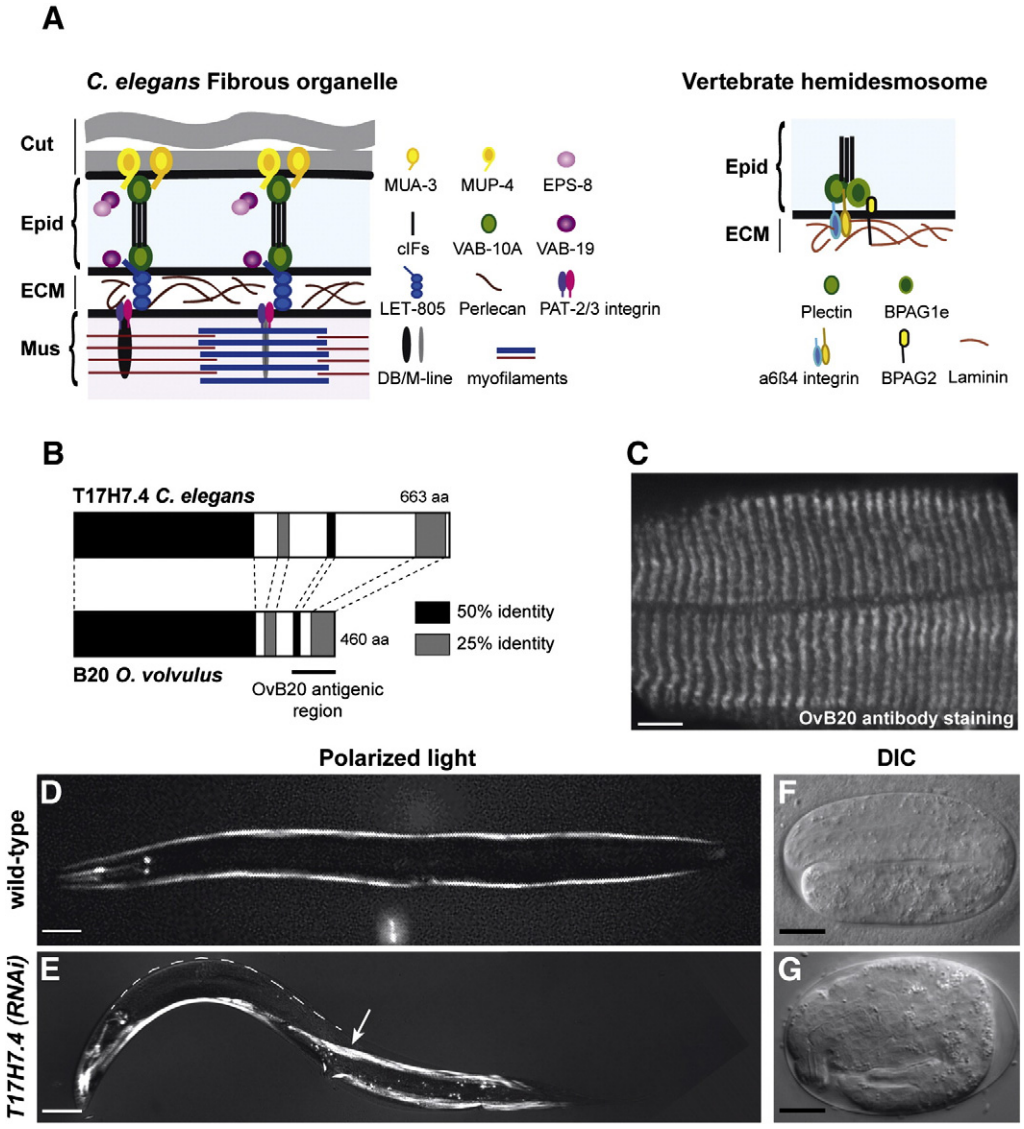

Fig. 1. Identification of *T17H7.4* in a search for potential anti-nematode targets. (A) Schematic comparison between *C. elegans* fibrous organelles (left) and vertebrate (right) hemidesmosomes. The main differences between them are the presumptive transmembrane receptors: nematode-specific transmembrane domain proteins with EGF (MUA-3 and MUP-4 apically) or FNIII (LET-805 basally) repeats, versus the α6ß4-integrin in vertebrates. Additional CeHD components include the Ankyrin-repeat protein VAB-19 (similar to Kank) and a probable VAB-19 interactor similar to the signalling adaptor protein Eps-8 (Ding et al., 2003, 2008). Cut, cuticle; Epid, epidermis; Mus, muscle. (B) *C. elegans* T17H7.4A and *O. volvulus* B20 protein identity. Black and grey boxes represent 50% identity and 20% identity, respectively. (C) OvB20 antibody staining on an adult wild-type N2 focusing on FOs (scale bar, 10 μm). (D–E) Polarized light pictures on wild-type (D) and *T17H7.4 (RNAi)* adults (E) showing muscle detachment (arrow) in RNAi-treated animals (scale bars, 50 μm). (F-G) DIC pictures of wild-type (F) and *T17H7.4(RNAi)* treated animals (G). Scale bars: 50 μm (C–D), 10 μm (E–F).

Materials and methods

C. elegans culture and strains

Control N2 and other strains were grown on NGM plates seeded with OP50 *Escherichia coli* at 20 °C unless otherwise stated (Brenner, 1974). The following alleles were used: *pat-12(st430)* and *pat-12(tm2298)*, which were outcrossed seven times against N2 and maintained in trans to the balancer *sC1(s2023)[dpy-1(s2170)]*; *vab-10(h1356)*; *vab-10A(e698)*; as well as the strains EE86 *mup-4(mg36) III;mupIS1[mup-4::GFP; pRF4 (rol-6)]* and *ML1050 mcIs44[lin-26p::vab-10$_{ABD}$::mcherry, myo-2p-GFP] IV*.

RNA interference (RNAi)

RNAi by feeding was carried out on NGM plates supplemented with 1mM IPTG and 100 μg/ml carbenicillin, using clones from the Ahringer-MRC library (Kamath et al., 2003). An RNAi feeding vector for *T17H7.4* was created by amplifying a 925 bp region spanning the 3' end of *T17H7.4* coding sequence using the primers 5'-aagaacgtcgtagccgtcat and 5'-actcttgggttgcttcgttg. The resulting PCR product was cloned into the plasmid L4440 (Addgene), which was transformed into electro-competent HT115(DE3) *E. coli*. RNAi-inducing bacteria were grown overnight at 37 °C and induced with 1mM of IPTG before being spread on plates. Wild-type N2 animals were prepared by alkaline hypochlorite treatment of gravid adults and the resultant L1 larvae were placed on freshly seeded RNAi plates; phenotypes were recorded 3 and 4 days later. Double stranded RNA (dsRNA) for injection was generated using the Ambion mMessage mMachine kit as described elsewhere (Bosher et al., 2003), and injected into young adults. Injected animals were allowed to recover overnight, then allowed to lay eggs for 1 h; their semi-synchronized progeny were examined for phenotypes or stained within the same day.

Yeast two-hybrid screen

We utilized a stringent version of the two-hybrid system that expresses baits and prey from low copy number plasmids. This system uses the three reporter genes *GAL1::HIS3*, *GAL1::lacZ* and *SPAL10::URA3* to test for an interaction compared with controls, as described (Vidal, 1997; Walhout and Vidal, 2001). The region encoding VAB-10 residues 408–1363 was cloned into the Gateway® yeast expression vector pPC97-Dest, as described (Hartley et al., 2000; Walhout et al., 2000). The resulting DB-ORF plasmid was transformed into the yeast strain Mav203. Auto-activation was tested by testing the activation of *GAL1::HIS3* on minimal medium lacking histidine but containing 20 mM 3-amino-1,2,4-triazole (3-AT) in the absence of any AD-containing vector, as described (Walhout and Vidal, 2001). The bait strain containing the VAB-10-DB fusion was transformed with the *C. elegans* AD-CecDNA library (Walhout et al., 2000), as described (Walhout and Vidal, 2001), in order to obtain 1.5 x 10^6 double transformants. After 4–5 days at 30 °C, single 3-AT resistant colonies were picked onto synthetic complete medium lacking Leu, Trp, and His and containing 20 mM 3-AT and then re-arrayed on similar fresh selective medium. Finally, the VAB-10(408–1363)–GEI-16 interaction was retested by gap repair in fresh Mav203 containing the VAB-10(408–1363)–DB fusion, as described (Walhout and Vidal, 2001). To determine which region of VAB-10A is involved in the interaction with GEI-16, we generated VAB-10A–DB deletion plasmids. The following VAB-10A amino acids corresponding sequences were introduced in pDest32 (Invitrogen) to generate the different spectrin repeat deletions: Spec1–2 (408–743), Spec1–3 (408–986), Spec1–5 (408–1218), Spec6 (1211–1363), Spec5–6 (1102–1363), Spec4–6 (980–1363), Spec3–6 (737–1363), Spec1 (408–632), Spec2 (632–743), Spec3 (746–986). The VAB-10A–DB deletion plasmids were then individually transformed with a GEI-16A–AD construct corresponding to the amino acids (30–243) introduced in pDest22 (Invitrogen). Positive interactions were selected for on minimal medium lacking Leu, Trp and His but containing 20 mM 3-AT. After 4–5 days growth at 30 °C, single 3-AT resistant colonies were picked and re-arrayed on similar fresh selective medium. In addition, these positive interactions were confirmed by testing for the activation of the *GAL1::lacZ* and *SPAL10::URA3* promoters as described in (Walhout and Vidal, 2001).

Cell cultures, transfections and co-IPs

VAB-10-HA was produced by amplifying the region encoding the plakin domain (amino acids 530–1363) with a 3' primer containing an HA tag. PAT-12-FLAG was produced by amplifying the region corresponding to the Y2H clone (see above) with a 3' primer containing a FLAG tag. Each PCR product was inserted in the pcDNA3 vector (Invitrogen).

HeLa cells (American Type Culture Collection, Rockville, MD, USA) were grown in Dulbecco's modified Eagle's medium (DMEM) supplemented with 5% foetal bovine serum and 1% gentamycin. 1.8 x 10^6 cells were plated on a six-well plate (300 000 cells per well) and maintained in an incubator at 37 °C with 5% CO_2 for 24 h. HeLa cells were then transfected with 1 μg/well of each plasmid using JetPEI™ reagent from Polyplus Transfection™, and cultured for 24 h post-transfection. Cells were then collected in cold 1× PBS and lysed in 300 μl cold lysis buffer (50 mM Tris–HCl pH 7.4, 150 mM NaCl, 1 mM EDTA, 1% Triton X-100 supplemented with Protease Inhibitor Cocktail (Roche)) for 15 min on ice. Cell lysates were centrifuged for 30 min at 14 000 rpm at 4 °C. 50 μl of the supernatant were kept for the input control and supplemented with 16.6 μl of 4× loading buffer. The remaining 250 μl were added to the anti-FLAG M2 Affinity Gel (Sigma) and incubated overnight at 4 °C on a rocking machine. The gel was rinsed three times with lysis buffer and resuspended in 150 μl of 1× loading buffer. Samples were electrophoresed on 12.5% SDS–polyacrylamide gels and transferred onto nitrocellulose membranes. Membranes were blocked for 1 h at room temperature in blocking buffer (1× PBS, 0.01% Tween-20 containing 3% non-fat milk powder), and then incubated overnight at 4 °C with anti-FLAG or anti-HA HRP-conjugated antibodies, both diluted 1:2000 in blocking buffer. Membranes were washed five times in 1× PBS/0.01% Tween-20 for 5 min, and resolved by chemi-luminescence (Immobilon™ Western HRP substrate, Millipore).

pat-12/T17H7.4 cDNAs and reporter constructs

cDNAs

T17H7.4 cDNAs were made by RT-PCR using SuperScript® II Reverse Transcriptase (Invitrogen) on both mixed stage and embryonic RNA samples. A common reverse primer was made for all isoforms and specific primers were made to all putative ATGs. Subsequently cDNAs were cloned into pGEM®-T Easy by AT-cloning.

GFP reporters

All reporter constructs were created by PCR with Expand Long Taq DNA Polymerase (Roche; amplicons greater than 5 kB) or HiFi PCR (Stratagene; amplicons less than 5 kB). Promoters for transcriptional GFP reporters were created by amplifying genomic DNA from the cosmid *T17H7* with the following primers: construct A, 5'-accggtctgcaaacccttcctgtagc and 5'-accggtcgtcgaccaatatgttttttgagc; construct J, 5'-accggtcgagtgcctgcaattgtct and 5'-accggtgctccgagttga-gaaactttg; construct K, 5'-accggtcaagtttcctgaaaatgctcct and 5'-accggtgttgcgcctgggattttac. PCR products were inserted at the AgeI site of the vector pPD95.75 (Addgene). Translational GFP reporters were created by PCR of promoters (see above) and cDNAs; promoters were directionally cloned into pPD95.75 with SphI and KpnI enzymes; cDNAs were placed between promoters and the GFP coding sequence by digestion with AgeI. The translational GFP reporter for isoforms E/F/I was created by PCR fusion, using a promoter PCR product and a GFP PCR product using the primers 5'-tgcaatacgtccacctgaaa and 5'gagtcgacctgcaggcatgcaagctacgacgacgtc-tatcatcattcag (promoter and coding sequence), 5'-agcttgcatgcctg-caggtcgact and 5'-tctgtgcggtatttcacacc (GFP coding sequence and *unc-54* 3'UTR from the plasmid pPD95.75). The final product was

generated using the primers 5'-cgggtactccaggttttcaa and 5'-aagggcc cgtacggccgactagtagg.

Transgenic animals

Constructs were injected into N2 young adults at a concentration of 10 ng/μl with 100ng/μl of the dominant *rol-6* containing plasmid pRF4 [rol-6(su1006)] as an injection marker and pBSKII at 90 ng/μl. An average of 10 lines were examined to select the best lines (most stable, least mosaic and best signal) which correspond to the following transgene names for each isoform : *mcEx534* for *gei-16A*, *mcEx537* for *gei-16K*, *mcEx538* for *gei-16J* and *mcEx539* for *gei-16E*. Rescue was assayed after injection into *pat-12(tm2298)/sC1(s2023) [dpy-1(s2170)]* animals. The *gei-16A::GFP* transgene generated in the *pat-12* mutant background corresponds to *mcEx535*.

Scoring lethality and DIC phenotypes

To determine embryonic lethality approximately 20 mothers were placed on a plate with a fresh and small bacterial spot and allowed to lay eggs for a few hours. Mothers were removed, embryos were counted at 8 h and 24 h after egg-laying. When scoring rescue by transgenes, the proportion of fluorescent embryos or larvae was also determined 24 h post-laying under a Leica MZIII fluorescence stereomicroscope. For DIC, animals were mounted in M9 buffer and examined under a Zeiss Axioplan microscope. In some cases, animals were also examined under polarized light after anesthetising larvae with 0.1% sodium azide in M9 buffer.

Immunofluorescence

Embryos and larvae and adults were fixed and stained by indirect immunofluorescence as described elsewhere (Bosher et al., 2003). The MH4, MH46 and MH3 monoclonal antibodies (Developmental Studies Hybridoma Bank, University of Iowa) (Francis and Waterston, 1991) and the NE8/4C6 mAb (Medical Research Council) (Schnabel, 1995) were diluted 1:250; the rabbit antisera against VAB-10A (4F2) (Bosher et al., 2003), and GFP (Roche) were diluted 1:1000. The OvB20 antibody was the kind gift of Dr. Wang Yu and used at a dilution of 1:100. Primary antibodies were detected using Cy3- or FITC-conjugated secondary antibodies. Stacks of images every 0.3 μm were captured using a confocal microscope (Leica SP2 AOBS/IRBE or Leica MP5 confocal microscope); approximately 10 confocal sections were projected using image J software and then processed using Adobe Photoshop®. Hoechst 33258 staining was performed as previously described (Moribe et al., 2004).

Electron microscopy

Embryos and larvae were fixed by High Pressure Freezing using a Leica Empact2. Freeze substitution was performed in the Leica EM AFS for 60 h at −90 °C in 2% osmium tetroxide 0.25% uranyl acetate/ 0.5% glutaraldehyde/1% H_2O in pure acetone. Temperature was raised to −30 °C at a 3 °C/h rate; samples were incubated for 12 h at −30 °C in pure acetone, then infiltrated in a graded concentration of epon–araldite resin mix (Sigma). Pictures were acquired using a FEI Morgagni transmission electron microscope operated at 70 kV.

Results

T17H7.4 identification

We identified *T17H7.4* in a bioinformatic search for nematode-specific genes (Fig. S1), with a predicted essential function, that could become novel drug or vaccine targets for treatment of infections with parasitic nematodes (Behm et al., 2005). The gene *T17H7.4* attracted our attention for two reasons. First, it encodes several isoforms with strong homology to antigen B20 from the filarial nematode *Onchocerca volvulus* (Fig. 1B) (Abdel-Wahab et al., 1996), which partially protects different hosts against infection when used for immunization (Graham et al., 2000; Taylor et al., 1995). Second, *T17H7.4* from *C. elegans* was identified in a yeast two-hybrid screen against the Rac regulator GEX-3 (Tsuboi et al., 2002) but was not characterized beyond showing that the gene is probably essential.

To define at what stage *T17H7.4* is essential, we repeated the RNAi tests performed by Tsuboi and colleagues (Tsuboi et al., 2002). Using RNAi feeding on young L1 larvae, we found that by the time control animals had reached the adult moult, 40% of *T17H7.4(RNAi)* animals were dead ($n = 600$), often with moulting problems, and the remainder were paralysed due to detached muscles (Fig. 1E; Fig. S2B). Furthermore, *T17H7.4(RNAi)* larvae could uptake Hoechst dye without any prior permeabilisation, which is indicative of a defective cuticle (Fig. S2D). Paralysis combined with moulting defects could mean that this gene acts in muscles and the epidermis. Alternatively, it could primarily reflect a FO defect in all muscle-cuticle anchoring structures. Consistent with the latter possibility, an antibody against the OvB20 antigen

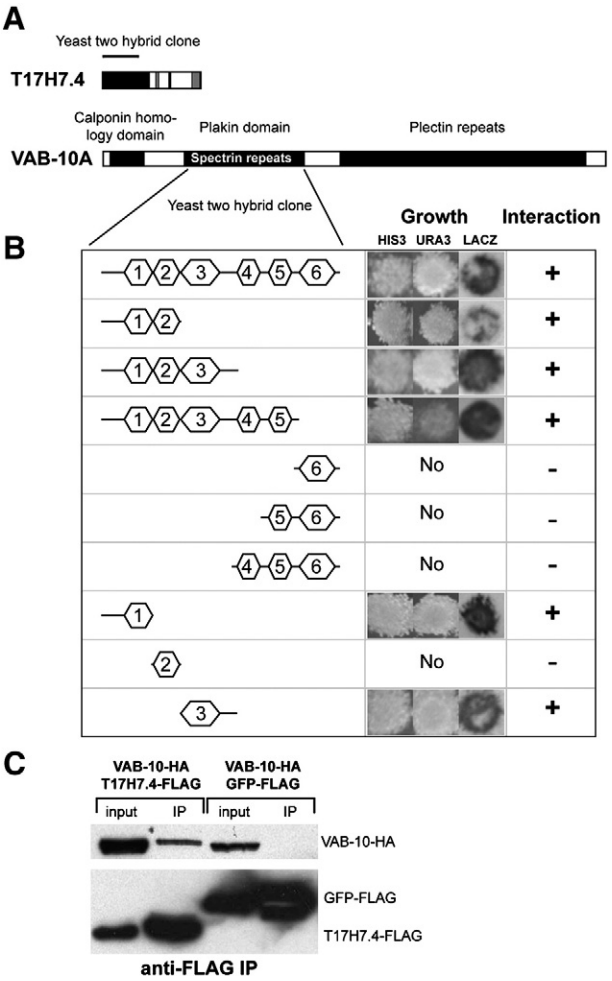

Fig. 2. Identification of T17H7.4 in a search for potential VAB-10A interactors. (A) Schematic representation of T17H7.4 (upper part; see Fig. 1) showing the position of the yeast two-hybrid clone identified in a screen against the plakin domain of VAB-10A (lower part). This plakin domain contains six spectrin repeats (see part B). (B) Yeast two-hybrid experiment between different variants of the six plectin domains of VAB-10A (bait) and a fragment of T17H7.4 (prey; see Fig. 3 for details). The yeast two-hybrid interaction was tested by evaluating the expression of three different genes: HIS3, URA3 and LacZ on appropriate media. (C) Co-IP experiment between the six plectin domains of VAB-10A tagged with an HA tag and a fragment of T17H7.4 (same fragment as used for the yeast two-hybrid screen) tagged with a FLAG tag. The co-IP was performed using an anti-FLAG antibody. As a control, GFP tagged with a FLAG tag was used to co-IP VAB-10A.

(Abdel-Wahab et al., 1996) decorated *C. elegans* larvae with a distribution characteristic of CeHDs (Fig. 1C).

To confirm the possibility that T17H7.4 could primarily affect CeHDs, we injected *T17H7.4* dsRNA into young adults to observe embryonic phenotypes (RNAi-treated larvae produced too few progeny). We observed that most embryos failed to undergo proper morphogenesis (95%), and arrested prior to the two-fold stage with thin head and tail (Fig. 1G), barely moving within the eggshell. This phenotype is strikingly reminiscent of that observed in mutants lacking one of the essential CeHD components, such as LET-805, VAB-10A, VAB-19, EPS-8, IFB-1A, IFA-3 (Bosher et al., 2003; Ding et al., 2003, 2008; Hapiak et al., 2003; Hresko et al., 1999; Woo et al., 2004).

On the other hand, we independently identified T17H7.4 in a yeast two-hybrid screen using as bait the central VAB-10 plakin domain, which consists of six spectrin repeats (Fig. 2A). Out of 10^6 colonies screened on selective medium, we identified 26 candidate VAB-10 partners, two of which encoded the N-terminal region of T17H7.4 (Fig. 2A; a full list of candidates is the focus of another study to be presented elsewhere). We further refined the VAB-10 region that potentially binds to T17H7.4 to the first and third spectrin domains (Fig. 2B). We also observed that the T17H7.4 clone recovered in the yeast two-hybrid screen could interact with itself if T17H7.4–LexA DNA-binding and T17H7.4–GAL4-activation fusion constructs were co-transformed in yeast (data not shown). To confirm the VAB-10A–T17H7.4 potential interaction, we expressed the first 243 residues of T17H7.4 tagged with FLAG, and the VAB-10 plakin domain tagged with HA in HeLa cells, and tested whether we could co-immuno-precipitate (co-IP) the two proteins. As shown in Fig. 2C, an antibody against FLAG could immuno-precipitate both VAB-10-HA and T17H7.4-FLAG, whereas it did not precipitate VAB-10-HA from cells co-expressing VAB-10-HA and FLAG-GFP.

Taken together, the biochemical interaction between T17H7.4 and VAB-10, the subcellular localisation of the OvB20-related antigen and the phenotype observed after RNAi against *T17H7.4* indicate that it might encode a novel hemidesmosome component.

T17H7.4 corresponds to the gene pat-12

To confirm the phenotype observed after *T17H7.4(RNAi)*, we examined the phenotype of the deletion allele *T17H7.4(tm2298)* recently produced by the National BioResource Project (Japan). *T17H7.4* is a complex gene predicted by Wormbase to generate 27 isoforms, many of which we confirmed in our own RT-PCR experiments (Fig. 3A). The allele *T17H7.4(tm2298)* is likely to be a null or a very strong loss-of-function allele, as it deletes part of exon 17 plus exons 18–19, which would induce a premature stop in intron 19, thus truncating all isoforms (Fig. 3A). All homozygous *tm2298* embryos died with a phenotype indistinguishable from that observed after *T17H7.4(RNAi)* (Fig. 3C). Injecting *T17H7.4* dsRNA into *T17H7.4(tm2298)/+* mothers did not aggravate the phenotype observed for *tm2298*, which provides further indication that it is a probable null allele (data not shown).

Looking at the genetic map of chromosome III where *T17H7.4* is located, we noticed two genes with predicted roles in embryonic morphogenesis and muscle anchoring, *pat-4* and *pat-12* (Williams and Waterston, 1994). The gene *pat-4* is required for anchoring myofilaments to the muscle plasma membrane and encodes the *C. elegans* ILK homolog (Mackinnon et al., 2002). The gene *pat-12* might also be involved in anchoring muscles to the epidermis (Williams and Waterston, 1994), but its function has not yet been characterized molecularly. Embryos homozygous for *pat-12(st430)* could elongate until slightly beyond the two-fold stage; they initially exhibited occasional twitching

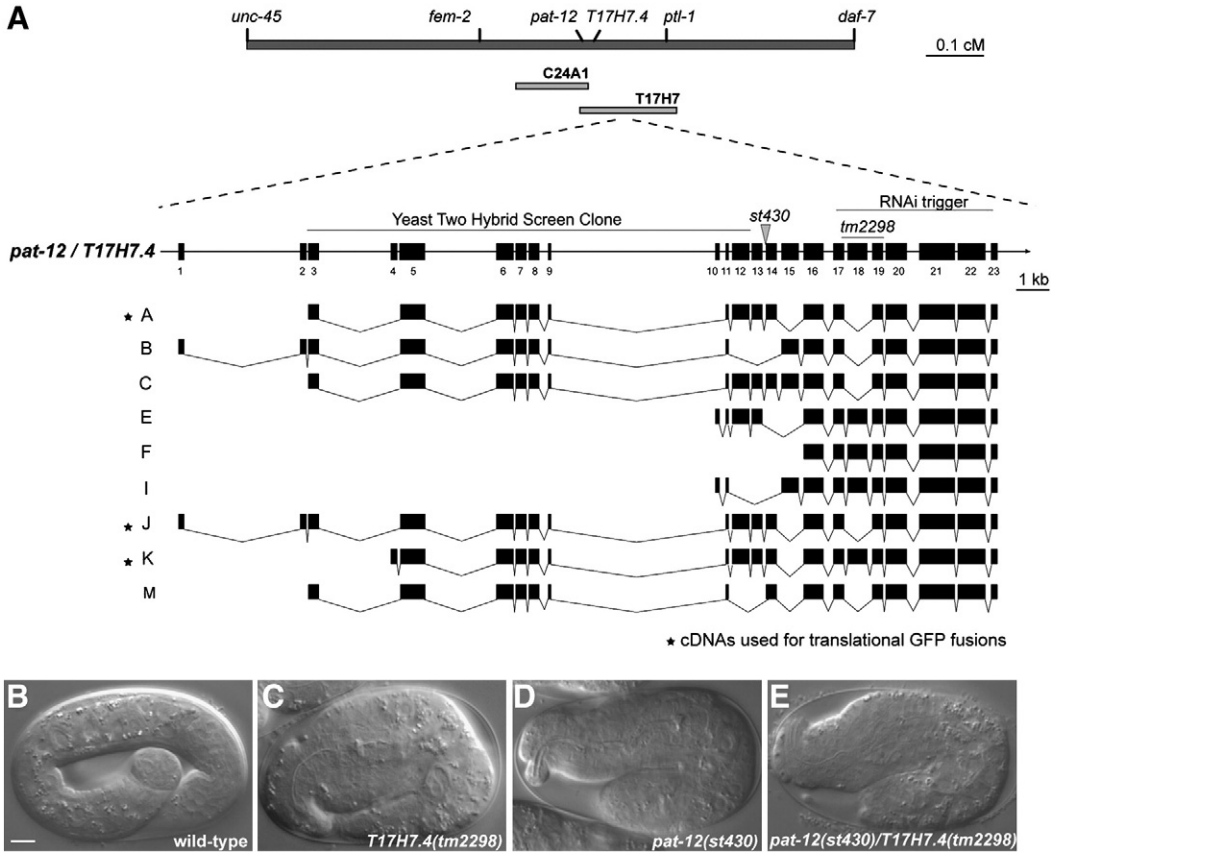

Fig. 3. *T17H7.4* corresponds to *pat-12*. (A) Genetic map and gene organisation of the *pat-12/T17H7.4* locus. The positions of *pat-12* alleles, or the region targeted for RNAi and of area encoding the VAB-10B-interacting clone are shown. The cDNAs represented are those we could confirm by RT-PCR. Note that isoforms B and C differ from isoform A by alternative exons located beyond the most conserved region of the gene. (B–E) DIC pictures of wild-type (B), *pat-12(st340)* (C), *pat-12(tm2298)* (D), *pat-12(st340)/pat-12(tm2298)* (E) embryos. For B, C, D and E, scale bar, 5 μm.

and gentle rolling in the eggshell, but soon ceased all movements (Fig. 3D). To test whether *T17H7.4* might correspond to *pat-12*, we sequenced the allele *pat-12(st430)* and tested whether it complements *T17H7.4(tm2298)*. We found that *pat-12(st430)* is a G to A transition in the AG splice acceptor of *T17H7.4* exon 14 (Fig. 3A), which should create a frameshift if exon 14 splicing is skipped. Furthermore, *pat-12(st430)* failed to complement *T17H7.4(tm2298)*, producing embryos with a phenotype intermediate between those induced by *st430* and *tm2298* alone (Fig. 3E). Consistent with the observation that *st430* results in a phenotype less severe than *tm2298*, only four of the nine *T17H7.4* transcripts that we confirmed contain exon 14. Hence our molecular and genetic data support the conclusion that *T17H7.4* corresponds to *pat-12*. Below we will refer to *T17H7.4* as *pat-12*, as the name was coined earlier (Williams and Waterston, 1994).

We found no significant PAT-12 homologues outside of the Nematoda phylum, suggesting that this locus arose in nematodes only. Among nematodes, many parasitic and free-living species, including nematodes from clades I, III, IV and V (sequence information was not available for clade II) contain a *pat-12* homologue (Fig. S1). Conservation is confined to the N-terminal half of the longest isoforms A, J, and K (Figs. 1 and 3). The different PAT-12 isoforms display no obvious homology to any known domains according to *InterProScan*.

Distribution of PAT-12A, E, J, K isoforms: PAT-12A and J are fibrous organelle components

To define the expression patterns of *pat-12* isoforms, we used GFP translational fusions. Since *pat-12* contains four large intronic regions before the predicted ATG corresponding to isoforms A, K, D, E/F/I, we assumed that these introns may represent different promoters.

To define the subcellular localization of PAT-12 isoforms, we used the immediate upstream intron as a potential promoter to control the expression of a cDNA (isoforms J, A and K) or genomic DNA (isoform E/F/I; Fig. 4A). We found that isoforms J and A had a distribution characteristic of pharyngeal and epidermal FOs, respectively (Fig. 4B–F). Specifically, PAT-12J was present at the basal and apical plasma membranes of the pharynx, like the plakin VAB-10A, whereas PAT-12A also colocalized with cIFs in the epidermis, forming parallel bands (Figs. 4B and 5A–B). In addition, PAT-12J::GFP appeared to be expressed in a punctate manner that might indicate co-localization with cIFs or aggregation (Fig. 4B–D). During late stages of embryogenesis, PAT-12K colocalized with junctions between seam and other epidermal cells (not shown) and formed circumferentially oriented bands in seam cells (Fig. 4B, G). As revealed by co-expressing PAT-12K::GFP with the actin-binding reporter VAB-10_{ABD}::mCherry (Gally et al., 2009), this bundle pattern appeared to partially coincide with actin, although the circumferentially oriented seam microfilament bundles highlighted by mCherry started to fade away before overlapping the PAT-12K::GFP signal (Fig. 4G-I). Thus, the nature of the PAT-12K filaments remains uncertain. In larvae, PAT-12K distribution was quite similar to that of PAT-12A in the epidermis, though much fainter (data not shown). The isoforms PAT-12E/F/I were detected in the spermatheca, where they marked the plasma membrane, and very weakly in the vulva (Fig. 4B, J, K).). In conclusion, although PAT-12 expression appears quite complex, our expression studies support the notion that *pat-12* defines a novel component of FOs, and raises the possibility that PAT-12 isoforms are present where cIFs are located.

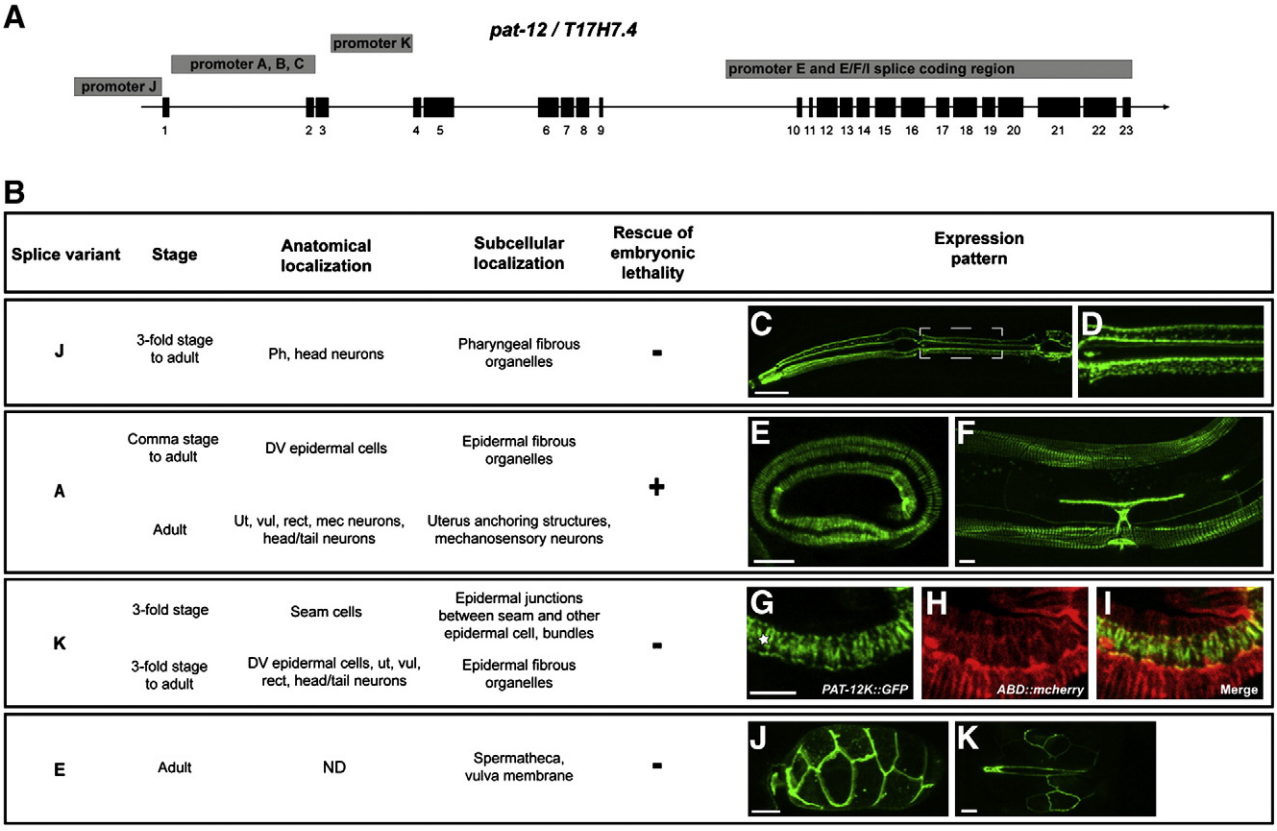

Fig. 4. PAT-12 isoforms associate with hemidesmosomes and filamentous structures. (A) Schematic representation of the genomic region used to generate GFP fusions. In each case the GFP was positioned at the C-terminal of the protein. (B) Summary table of the pattern of expression of the transcriptional (anatomical localization) and translational (subcellular localization) fusions for the different variant tested. Ph, Pharynx, DV, dorso-ventral, ut, uterus, vul, vulva, mec, mechanosensory, rect, rectum. (C–K) Confocal pictures of the different translational fusions expressed in the wild-type and presented in B. (C, D) Pharynx of an L4 stage expressing the J::GFP translational fusion. D represents a high magnification picture of the region highlighted by the dashed rectangle in C. (E, F) A::GFP translational fusion expressed in embryo (E) or adult (F). (G–I) Coexpression of K::GFP translational fusion (G) and ABD::mcherry (H) in an embryo showing partial overlap of both markers (I) in the seam cells (star in G). (J, K) E::GFP translational fusion expressed in the spermatheca filled with an egg (J) and in the vulva (K) in the adult. Scale bars, 10 μm for C, D, E, F, J and K and 5 μm for G–I.

The PAT-12A isoform is critical to ensure viability

To define whether any isoform is essential for viability, we used the translational fusion constructs described above to test whether they could rescue the lethality of the null allele *pat-12(tm2298)*. Expression of isoforms J, K, or E/F/I could not rescue embryonic lethality (Fig. 4B). Conversely, expression of isoform A rescued most *pat-12(tm2298)* embryos, and a stable homozygous *pat-12(tm2298)* mutant transgenic line could be maintained (Fig. 4B). Homozygous *pat-12(tm2298)* expressing *pat-12A::GFP* segregated about 69% fluorescent animals that could reach adulthood with a growth rate undistinguishable from the wild-type growth rate (N=154). The remaining 31% fluorescent embryos developed beyond the three-fold stage but could not hatch, probably due to mosaic inheritance of the transgene. This observation shows that the A isoform is essential for function, and further suggests that PAT-12 function is dispensable for feeding, fertilization and egg-laying.

PAT-12A is essential for fibrous organelle biogenesis

Having established that PAT-12A is a novel fibrous organelle component, and that it is essential for embryonic morphogenesis, we wished to assess whether its absence affects fibrous organelle biogenesis. To do so, we examined *pat-12(tm2298)* for potential CeHD and muscle defects.

Homozygous *pat-12(tm2298)* embryos had a normal distribution of muscles and CeHD components until the two-fold stage, when muscles start to actively twitch (Fig. S3). Subsequently, muscles detached from the body wall to collapse centrally, which was particularly obvious in the head and tail as well as in mid-body where the bend is more acute (Fig. 5E). Hence, muscles reach their normal positions, but cannot maintain them once they start to contract, which suggests that CeHDs are defective.

The distribution of UNC-52/Perlecan, a critical ECM component between muscles and the epidermis, and LET-805/myotactin, a probable UNC-52 receptor on the basal side of the epidermis, reflected the positions of muscles (Fig. 5G-J). It was normal until muscles started to twitch (not shown), and progressively disappeared from the anterior and posterior tips of the embryo. In the central part of the embryo, they remained apposed to muscles although LET-805 never formed characteristic parallel stripes (Fig. 5G-J). The distribution of VAB-10A/plakin showed the same trend, with two notable differences. First, since VAB-10A is normally associated with both the basal and apical membranes, two lines of staining in the same *Z*-plane could be transiently observed in *pat-12* mutants above each muscle quadrant at the time when control embryos reached the two-fold stage. We suggest that one line corresponds to the basal membrane, and the other to the apical membrane, suggesting that the epidermis widened and ruptured internally (Fig. 5E-F). Second, the apical signal became very faint, implying that it critically depends on PAT-12 for maintenance. Distribution of intermediate filaments was also abnormal, as epidermal

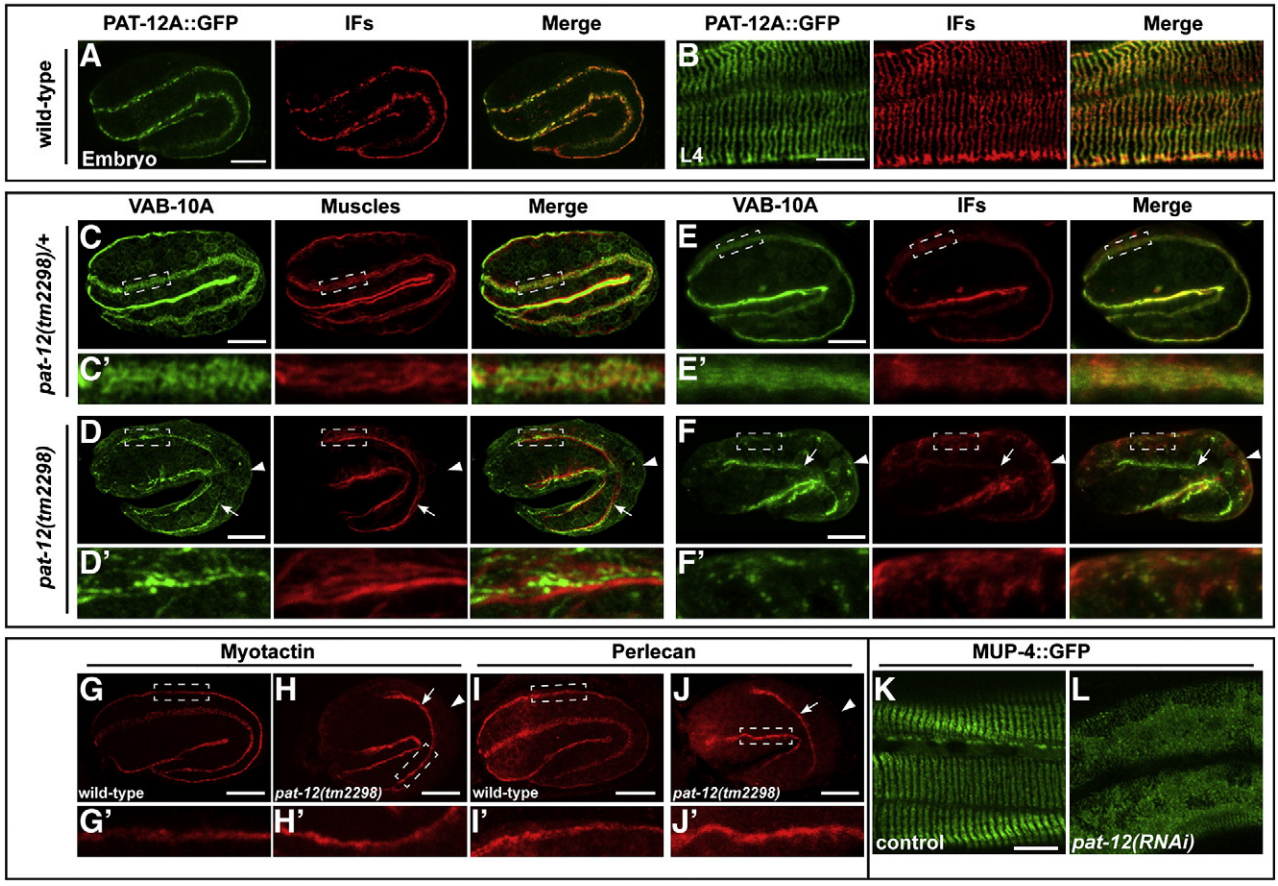

Fig. 5. Differential effect of PAT-12 loss on apical and basal hemidesmosomes. (A, B) Confocal pictures after immunostaining of PAT-12::GFP and IFs on a wild-type 1.8-fold embryo and L4 larvae showing a perfect overlap of the two colours. (C, E) Confocal pictures after immunostaining of VAB-10A and body wall muscles on *pat-12(tm2298)/sC1[dpy-1(s2170)]* heterozygous (C) and *pat-12(tm2298)* homozygous (E) embryos at the 2-fold stage. C' and E' represent high magnifications of the regions highlighted by the dashed rectangles in C and E, respectively. (D, F) Confocal pictures after immunostaining of VAB-10A and IFs(IFs) on *pat-12(tm2298)/sC1[dpy-1(s2170)]* heterozygous (D) and *pat-12(tm2298)* homozygous (F) embryos at the 2-fold stage. D' and F' represent high magnifications of the region highlighted by the dashed rectangles in D and F, respectively. Arrowheads point onto the possible apical surface of the epidermis. Arrows indicate detached epidermis and muscles. (G–J) Confocal pictures after immunostaining of LET-805/Myotactin (G, H) and UNC-52/Perlecan (I, J) on wild-type (G, I) and *pat-12(tm2298)* (H, J) 2-fold embryos. G'–J' represent high magnifications of the region highlighted by the dashed rectangles in G–J. K, L. MUP-4::GFP localization in a control (K) or *pat-12(RNAi)* (L) L4 larvae after confocal acquisition. For All panels, scale bars, 10 μm.

cIFs were mainly visible at the level of the apical plasma membranes (Fig. 5F), indicating that their integrity or attachment had been broken. Lastly, we examined the distribution of MUP-4, which acts together with MUA-3 as the putative apical ECM cuticle receptors (Bercher et al., 2001; Hong et al., 2001). We used *pat-12(RNAi)* feeding in larvae expressing MUP-4::GFP (MUP-4::GFP is difficult to see in embryos). We observed that MUP-4 staining faded away and became blurry in *pat-12(RNAi)* L4 larvae (Fig. 5L). Consistent with the genetic results described in Fig. 3, we observed similar, though weaker, defects in *pat-12(st430)* mutant embryos (data not shown). We conclude that PAT-12 activity is important to maintain FO integrity, and, might have distinct functions apically and basally, based on the differential loss of VAB-10A, cIFs and ECM receptors at the two plasma membranes.

Rupture of the epidermis and the ensuing muscle detachment could primarily result from a detachment of the epidermal plasma membrane from the extracellular matrix, or from a loss of FO integrity within the epidermis. To examine these possibilities, we examined the ultrastructure of PAT-12 defective animals by electron microscopy. After RNAi feeding in larvae, we observed a widening of the epidermis in L4 larvae (Fig. 6A–D) (80 ± 20 nm in control larvae, versus $1.6 \pm .2$ μm in *pat-12 (RNAi)* larvae, $N = 14$). Importantly, the apical plasma membrane was still associated with the cuticle and the basal plasma membrane still associated with the basal lamina (Fig. 6C, D). Likewise, in *pat-12 (tm2298)* embryos that had reached the equivalent of the two-fold stage, we observed a thickening of the epidermis (average 200 nm in controls to an average 1.2 μm in *pat-12(tm2298)* embryos, $n = 10$), yet plasma membranes were still associated with the extracellular matrices both apically and basally (not shown). Furthermore, the epidermis was the thickest where the muscles were located, and in several places it was sandwiched between muscles forming a spear shape (Fig. 6D). In conclusion, our EM and immunofluorescence data suggest that epidermal integrity is lost in *pat-12* mutants resulting from internal rupture, rather than rupture at the level of the plasma membrane or the ECM.

PAT-12A localization depends on other fibrous organelle components

One possible interpretation of the results described so far could be that PAT-12A links VAB-10A to the apical ECM receptor. Alternatively, it might interact with cIFs and potentially stabilize their interaction with VAB-10A/plakin, which is the most likely factor capable of anchoring them at CeHDs (Bosher et al., 2003). Lastly, it could have more than one role. A prediction of each scenario is that removing *vab-10A* or *ifb-1* might have different outcomes. For instance, if PAT-12A makes a complex with VAB-10A and IFB-1, loss of each protein could have similar consequences on PAT-12A distribution. Alternatively, if PAT-12A interacts with only VAB-10A, loss of cIFs would not affect its distribution, at least initially, until FOs fall apart due to loss of cIFs.

When we removed VAB-10A by RNAi, PAT-12A had a normal distribution until the 1.5-fold stage. Starting at the 1.8-fold stage, PAT-12A started to form dim and thin stripes apically in 57% of the animals (Fig. 7D, D', $n = 15$). In the remaining 43% of the animals observed, PAT-12A became fuzzy apically (Fig. 7E, E', $n = 9$). In all cases, PAT-12A formed disorganized aggregates basally (Fig. 7E and G). When we depleted IFB-1 by RNAi in embryos expressing PAT-12A::GFP, we observed that PAT-12::GFP could form stripes as observed in the *vab-10(RNAi)* background. However, these stripes were observed in most places of the embryo, except in the apical side of the bend past the two-fold stage (Fig. 7G) and in escaping arrested larvae (Fig. 7H). As a consequence, VAB-10 depletion had a more severe phenotype with respect to PAT-12A localisation that IFB-1 did, especially at the apical side. We conclude that PAT-12A::GFP distribution critically depends on VAB-10A and to a lesser extent on cIFs.

Discussion

Our studies show that PAT-12 defines a novel *C. elegans* hemidesmosome (CeHD) factor necessary to maintain the two core CeHD components, the plakin VAB-10A and cytoplasmic intermediate filaments (cIFs) (Fig. 8A). In addition, PAT-12 proved to be essential to maintain the proper distribution of the candidate apically localized CeHD ECM receptor MUP-4, but not of the candidate basally localized ECM receptor LET-805 (Fig. 8B).

PAT-12, a new component of the FO

Three lines of evidence strongly support that *pat-12* encodes a novel CeHD component. First, RNAi experiments and genetic analysis of *pat-12* mutants, including a presumptive null mutant, showed that *pat-12* is vital for nematode survival, causing paralysis and death in

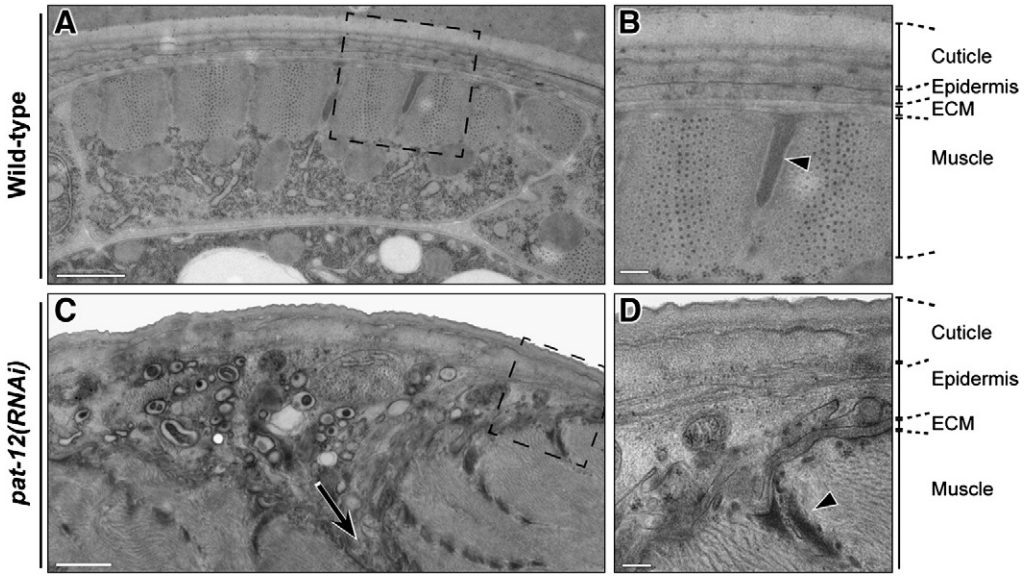

Fig. 6. PAT-12 knock-down leads to an epidermolysis bullosa simplex-like phenotype. EM pictures of wild-type (A, B, high magnification of A at the level of the dashed box) and *pat-12 (RNAi)* (C, D: high magnification of C at the level of the dashed box) adults showing muscle and epidermis structures. The relative positions of each structure are indicated through a legend on the far right. Arrow (in C), muscle detachment; arrowheads (in B, D), dense bodies. Scale bars, 1 μm in low magnification pictures and 200 nm in high magnification pictures.

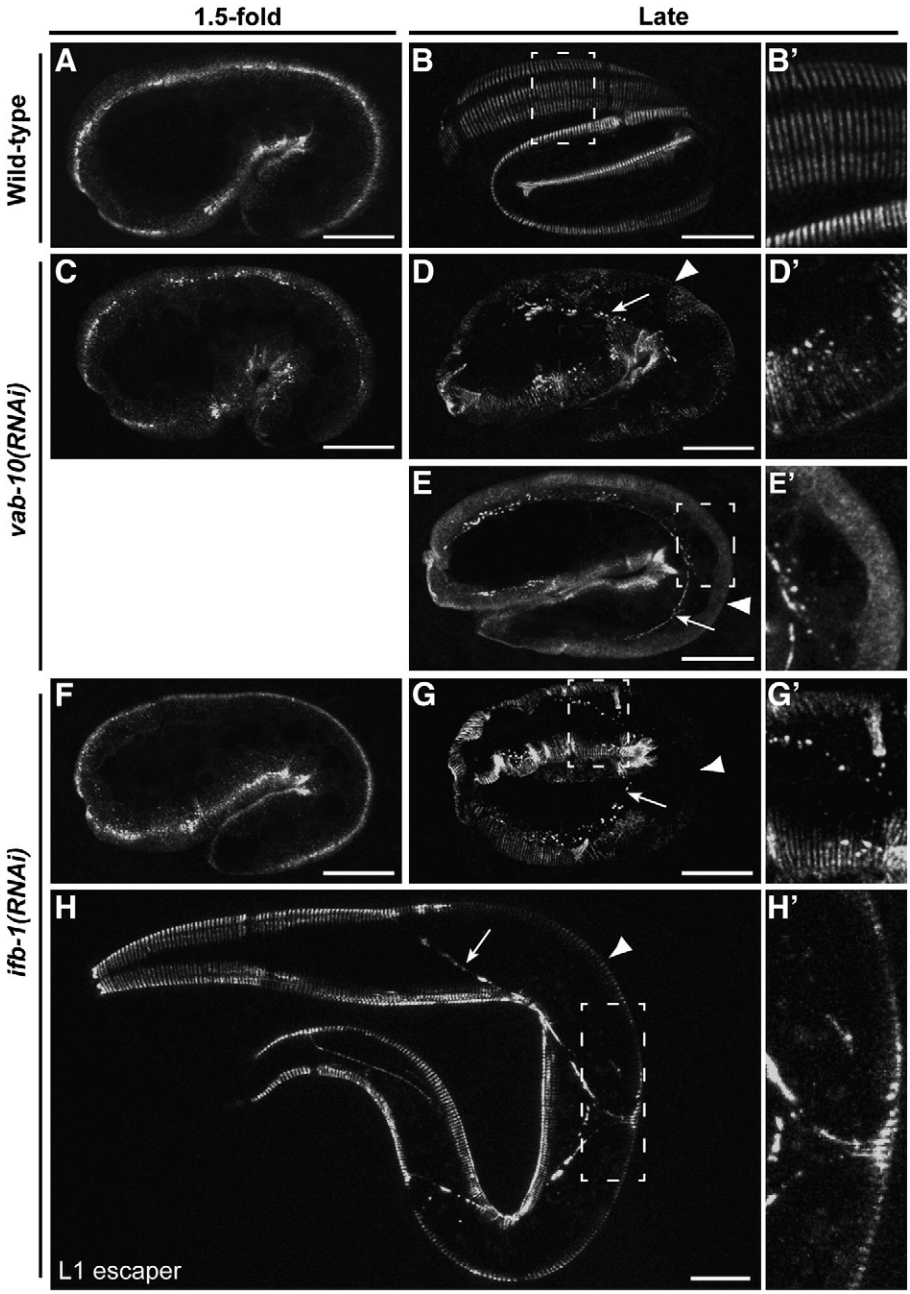

Fig. 7. PAT-12A localization depends on VAB-10A. PAT-12A::GFP localization in wild-type (A, B) *vab-10* RNAi-treated (C, D) and *ifb-1* RNAi-treated animals (E, F, G). (A, C, E) 1.5-fold embryos. (B, D, F) Late embryos corresponding to a 3.5-fold stage in wild-type and Pat in RNAi-treated animals. (G) L1 larva corresponding to an escape due to mild *ifb-1* RNAi effect. B'–G' correspond to high magnification pictures of the region highlighted with the dashed boxes in B–G. Arrowheads indicate apical surface of the epidermis and arrows point to the detached basal surface of the epidermis. Efficiency of the RNAi was as follows: *vab-10(RNAi)*, 98% embryonic lethal, *ifb-1(RNAi)*, 79% embryonic lethal and 19% larval lethal. For All panels, scale bars, 10 μm.

two-fold embryos, larvae and adults. This paralysis is due to muscle detachment from the body wall in embryos and larvae, a phenotype typical of CeHD mutants. Second, we found that the PAT-12A isoform has a characteristic CeHD distribution and colocalizes with epidermal cIFs. Furthermore, this isoform could rescue the lethality due to the putative null allele *pat-12(tm2298)*. Third, our characterization of *pat-12* mutants established that the apical and basal epidermal membranes separated from each other, and that several CeHD components could not be maintained. Electron microscopy (EM) confirmed that the epidermis adjacent to muscles was enlarged, but did not reveal a separation at the level of the epidermal plasma membrane. Typically, loss of the candidate apical CeHD ECM receptors MUP-4 or MUA-3 leads to detachment of the apical plasma membranes from the cuticle (Bercher et al., 2001; Hong et al., 2001). Similarly, loss of the plakin VAB-10A also increases the distance between the epidermis and the cuticle (Bosher et al., 2003). Loss of *pat-12* thus has a phenotype consistent with a failure of the cIFs to remain intact and resistant to stress. In vertebrates, it would qualify as an Epidermolysis Bullosa Simplex syndrome, rather than as a Junctional Epidermis Bullosa syndrome (Nievers et al., 1999).

The *pat-12* locus encodes several isoforms that are specifically expressed in most *C. elegans* epithelia, including the epidermal seam cells, the pharynx, the spermatheca, the vulva, the uterus and the rectum. Despite this widespread expression, our rescue experiments indicate that expression of PAT-12A, which is only present at the level of FOs, is sufficient to rescue the embryonic lethality of *pat-12(2298)* and generate viable and fertile animals. While it suggests that other isoforms are not critical for embryonic development and reproduction, we cannot

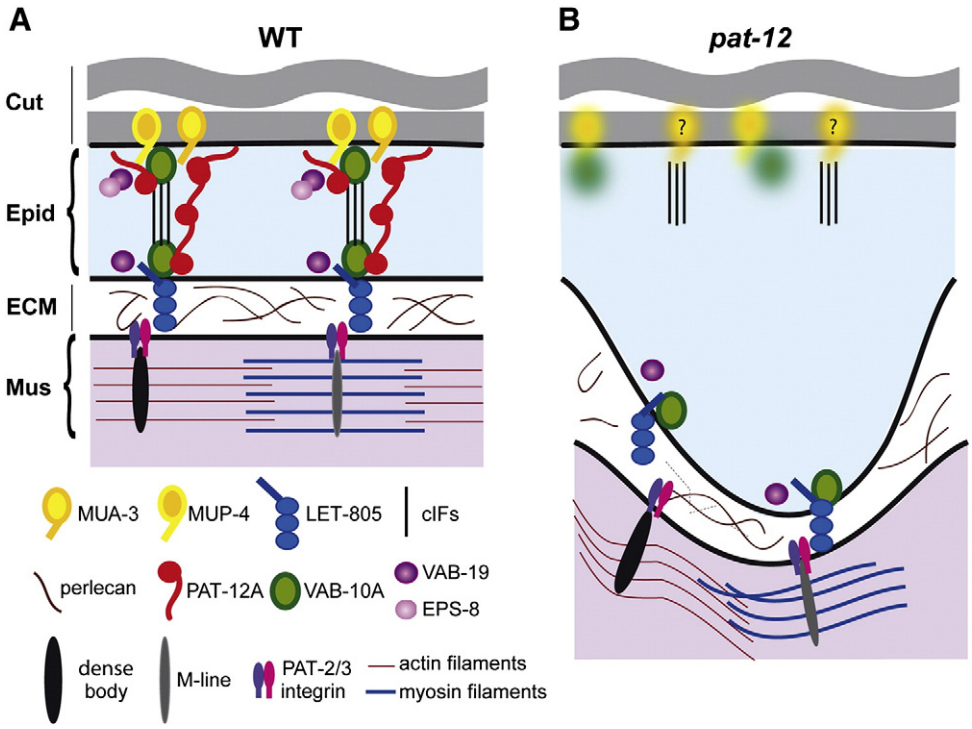

Fig. 8. Model for PAT-12A localization and function. The schematic drawing shows a transverse apico-basal section through the epidermis and muscle, highlighting the main hemidesmosome components in wild-type (A) and *pat-12* mutants (B). Note that a fibrous organelle corresponds to the apical and basal hemidesmosomes with their interconnecting intermediate filaments (cIFs). The question marks in (B) referrers to the potential mislocalization of MUA-3 in *pat-12* mutants that we did not test. See text for further details.

exclude that the other isoforms also help other epithelia resist shearing or stretching forces, perhaps redundantly with other proteins.

PAT-12 interaction with VAB-10A and possible molecular function

PAT-12 isoforms do not contain any protein domain that could provide hints for their role. Nevertheless, the distribution of PAT-12 isoforms, our biochemical analysis and the phenotypes of *pat-12* mutants offer indirect clues to their molecular function.

The different *pat-12* isoforms appear to have a dual distribution, since they localize to filamentous structures like fibrous organelles, but also to surrounding membranes of the pharynx, rectum, vulva and epidermis. For example, PAT-12K showed laterally oriented filaments that partially coincide with actin microfilaments. Two potential and non-exclusive mechanisms might account for PAT-12 localization. First, some or all isoforms could auto-assemble into filamentous multimers. Indeed, we did observe a PAT-12–PAT-12 interaction in yeast two-hybrid tests (data not shown), but we did not attempt to confirm it biochemically. Alternatively, PAT-12 isoforms could associate with specific junctional proteins and/or with other filamentous proteins. Our two-hybrid and biochemical data suggest that PAT-12 can interact with the VAB-10 plakin domain, and our genetic analysis indicates that in the absence of VAB-10A the distribution of PAT-12A::GFP becomes quite blurry in the epidermis. Hence, VAB-10 might anchor PAT-12A to CeHDs. The reports in mass yeast two-hybrid screens that PAT-12 can interact with four distinct cIFs (Li et al., 2004), which are yet to be confirmed, and the partial dependence of PAT-12A CeHD localization on IFB-1 might imply that PAT-12A can also directly associate with cIFs. However, PAT-12A::GFP maintained a fairly normal distribution in many places. Furthermore, loss of PAT-12A::GFP localization in some areas of IFB-1 depleted embryos might be indirect, since IFB-1 is required to maintain CeHDs (Woo et al., 2004). Hence, we do not presently favour the idea that PAT-12 localization and potential function results from a direct cIF–PAT-12 interaction.

In the absence of PAT-12, we observed three main phenotypes: (i) a progressive loss of VAB-10A from the apical membrane; (ii) a failure of cIFs to form the typical fibrous organelle repeated stripes and their apparent separation from the basal membrane; (iii) a blurry distribution of the putative apical ECM receptor MUP-4, but not of the putative basal ECM receptor LET-805 (Fig. 8B). Although CeHD integrity defects appear equally severe in *pat-12* and most other CeHD mutants, the specific *pat-12* cellular phenotypes set it apart, which helps define its potential function. For instance, cIFs aggregate in *vab-10A* mutants, whereas cIFs and VAB-10A maintain their banded pattern in *vab-19* mutants, although they extend beyond the muscle adjacent region (Bosher et al., 2003; Ding et al., 2003) (for a review, see (Zhang and Labouesse, 2010)). Based on our biochemical data, we propose that apically, PAT-12A presumably interacts with VAB-10A to maintain apical CeHDs and promote their assembly into regularly spaced parallel stripes. PAT-12A could stabilize the potential (and still hypothetical) VAB-10A interaction with MUP-4 and MUA-3, or else directly mediate VAB-10A interaction with MUP-4. The absence of PAT-12A could destabilize VAB-10A, leading to its loss and to the diffusion of MUP-4 within the apical plasma membrane. Basally, PAT-12A might also interact with VAB-10A, but assuming that VAB-10A also interacts with LET-805, this interaction could be stronger or less dependent on PAT-12A. Why would cIFs separate from the basal plasma membrane more readily than from the apical plasma membrane, given that the most obvious candidate for anchoring cIFs, the plakin VAB-10A (Bosher et al., 2003), is primarily lost from the apical membrane? First, this loss is progressive and the interaction between VAB-10A and cIFs basally might be more labile or might more critically depend on PAT-12A. Second, MUP-4 and MUA-3 have weak homology in their cytoplasmic domains with filaggrin (Hahn and Labouesse, 2001), a known intermediate filament binding protein, which might contribute to the retention of cIFs apically when VAB-10A disappears. In summary, we suggest that PAT-12A acts to stabilize the interaction of VAB-10A with other proteins.

PAT-12 as a potential drug target?

A major aim of this project was to characterise *pat-12* in order to assess its suitability as a drug target for parasitic nematodes. To qualify as an interesting drug target and merit further examination a number of criteria need to be satisfied. First, the target has an essential function in the relevant nematodes. Highly desirable loss-of-function phenotypes are lethality, especially in the parasitic stages of the life cycle, or paralysis, as many parasites once paralysed can be cleared by the host system, or sterility, which ensures that the next generation is not produced. PAT-12 is clearly essential in *C. elegans*, as absence of *pat-12* causes paralysis and lethality, at all stages of development. A second criterion is that the putative target has broad representation among relevant parasitic nematodes and good protein homology, such that a potential anthelmintic drug would potentially affect all economically important parasites. High protein sequence conservation maximizes the probability that the orthologous proteins in other species have a conserved structure that can be 'blocked' with a single drug. PAT-12 certainly appears to fulfil this second criterion: highly conserved PAT-12 homologs were found in most clades, allowing the *O. volvulus* antibody OvB20 to recognize a protein with a distribution very similar to that of PAT-12A. Finally, a potential drug target must have a 'druggable' structure.

Currently drugs are mostly designed by creating or discovering small molecules that can block the function of receptors or channels or fit into the binding pockets of enzymes (Behm et al., 2005; Pink et al., 2005). Although PAT-12 is essential in *C. elegans* and has orthologues in parasitic nematodes, it does not possess obvious domains for binding of small ligands. However, a structural analysis of PAT-12 might reveal domains that can be blocked by small components. Furthermore, we have established that VAB-10A co-operates with PAT-12, which is most likely achieved through creation of a complex. Disrupting this complex, or interfering with the activity of proteins that regulate the assembly of the putative PAT-12A/VAB-10A complex, would achieve the same end as blocking PAT-12 function, and creates a wider pool of possible proteins and pockets to block. Continued research into the regulation of cIFs and hemidesmosomes in *C. elegans* stands to benefit diverse areas of biology.

Supplementary materials related to this article can be found online at doi:10.1016/j.ydbio.2010.11.025.

Role of the funding sources

The work described in this paper was funded in part by Research and Development funds provided by Meat and Livestock Australia Ltd and Australian Wool Innovation Ltd. These funding bodies and the others listed below had no role in the design of the study, in the collection, analysis or interpretation of the data, in writing the manuscript or in the decision to submit the paper for publication.

CB was supported by Meat and Livestock Australia Ltd and Australian Wool Innovation Ltd (AHW.029). ML was supported by grants from the ANR (NT_NV_12) and ARC (4902 and 5055), and by institutional funds from the CNRS, INSERM and Université de Strasbourg.

SH was founded by the Australian government for an Australian Postgraduate Award, Meat and Livestock Australia Ltd (AHW.029) for a Junior Research Fellowship, the EMBO for a short-term fellowship, Development for a travel fellowship and travel grants, from the ARC/NHMRC Research Network for Parasitology and the Network in Genes and Environment in Development.

Acknowledgments

We are grateful to Shohei Mitani and the National BioResource Project (Japan) for the allele *tm2298*, the CGC for strains, Dr. Elizabeth Bucher (University of Pennsylvania, Philadelphia PA, USA) for the EE86 strain, Dr. Wang Yu (The Liverpool School of Tropical Medicine, Liverpool, UK) for the OvB20 antibody. We also thank Beena Jeevan for the FLAG-HA-GFP plasmid and Dr Arnaud Ahier for discussions and suggestions for Co-IP experiments. We acknowledge Huimin Zhang and Sophie Quintin for their careful reading of the manuscript.

References

Abdel-Wahab, N., Kuo, Y.M., Wu, Y., Tuan, R.S., Bianco, A.E., 1996. OvB20, an *Onchocerca volvulus* cloned antigen selected by differential immunoscreening with vaccination serum in a cattle model of onchocerciasis. Mol. Biochem. Parasitol. 76, 187–199.

Behm, C.A., Bendig, M.M., McCarter, J.P., Sluder, A.E., 2005. RNAi-based discovery and validation of new drug targets in filarial nematodes. Trends Parasitol. 21, 97–100.

Bercher, M., Wahl, J., Vogel, B.E., Lu, C., Hedgecock, E.M., Hall, D.H., Plenefisch, J.D., 2001. *mua-3*, a gene required for mechanical tissue integrity in *Caenorhabditis elegans*, encodes a novel transmembrane protein of epithelial attachment complexes. J. Cell Biol. 154, 415–426.

Bosher, J.M., Hahn, B.S., Legouis, R., Sookhareea, S., Weimer, R.M., Gansmuller, A., Chisholm, A.D., Rose, A.M., Bessereau, J.L., Labouesse, M., 2003. The *Caenorhabditis elegans vab-10* spectraplakin isoforms protect the epidermis against internal and external forces. J. Cell Biol. 161, 757–768.

Brenner, S., 1974. The genetics of *Caenorhabditis elegans*. Genetics 77, 71–94.

Butler, L.C., Blanchard, G.B., Kabla, A.J., Lawrence, N.J., Welchman, D.P., Mahadevan, L., Adams, R.J., Sanson, B., 2009. Cell shape changes indicate a role for extrinsic tensile forces in Drosophila germ-band extension. Nat. Cell Biol. 11, 859–864.

Chisholm, A.D., Hardin, J., 2005. Epidermal morphogenesis WormBook. http://www.wormbook.org. doi:10.1895/wormbook.1.7.1.

Ding, M., Goncharov, A., Jin, Y., Chisholm, A.D., 2003. *C. elegans* ankyrin repeat protein VAB-19 is a component of epidermal attachment structures and is essential for epidermal morphogenesis. Development 130, 5791–5801.

Ding, M., King, R.S., Berry, E.C., Wang, Y., Hardin, J., Chisholm, A.D., 2008. The cell signaling adaptor protein EPS-8 is essential for *C. elegans* epidermal elongation and interacts with the ankyrin repeat protein VAB-19. PLoS ONE 3, e3346.

Francis, R., Waterston, R.H., 1991. Muscle cell attachment in *Caenorhabditis elegans*. J. Cell Biol. 114, 465–479.

Gally, C., Wissler, F., Zahreddine, H., Quintin, S., Landmann, F., Labouesse, M., 2009. Myosin II regulation during *C. elegans* embryonic elongation: LET-502/ROCK, MRCK-1 and PAK-1, three kinases with different roles. Development 136, 3109–3119.

Graham, S.P., Lustigman, S., Trees, A.J., Bianco, A.E., 2000. *Onchocerca volvulus* comparative analysis of antibody responses to recombinant antigens in two animal models of onchocerciasis. Exp. Parasitol. 94, 158–162.

Hahn, B.S., Labouesse, M., 2001. Tissue integrity: hemidesmosomes and resistance to stress. Curr. Biol. 11, R858–R861.

Hapiak, V., Hresko, M.C., Schriefer, L.A., Saiyasisongkhram, K., Bercher, M., Plenefisch, J., 2003. *mua-6*, a gene required for tissue integrity in *Caenorhabditis elegans*, encodes a cytoplasmic intermediate filament. Dev. Biol. 263, 330–342.

Hartley, J.L., Temple, G.F., Brasch, M.A., 2000. DNA cloning using in vitro site-specific recombination. Genome Res. 10, 1788–1795.

Hong, L., Elbl, T., Ward, J., Franzini-Armstrong, C., Rybicka, K.K., Gatewood, B.K., Baillie, D.L., Bucher, E.A., 2001. MUP-4 is a novel transmembrane protein with functions in epithelial cell adhesion in *Caenorhabditis elegans*. J. Cell Biol. 154, 403–414.

Hresko, M.C., Schriefer, L.A., Shrimankar, P., Waterston, R.H., 1999. Myotactin, a novel hypodermal protein involved in muscle-cell adhesion in *Caenorhabditis elegans*. J. Cell Biol. 146, 659–672.

Kamath, R.S., Fraser, A.G., Dong, Y., Poulin, G., Durbin, R., Gotta, M., Kanapin, A., Le Bot, N., Moreno, S., Sohrmann, M., Welchman, D.P., Zipperlen, P., Ahringer, J., 2003. Systematic functional analysis of the *Caenorhabditis elegans* genome using RNAi. Nature 421, 231–237.

Keller, R., 2006. Mechanisms of elongation in embryogenesis. Development 133, 2291–2302.

Lecuit, T., Le Goff, L., 2007. Orchestrating size and shape during morphogenesis. Nature 450, 189–192.

Li, S., Armstrong, C.M., Bertin, N., Ge, H., Milstein, S., Boxem, M., Vidalain, P.O., Han, J.D., Chesneau, A., Hao, T., Goldberg, D.S., Li, N., Martinez, M., Rual, J.F., Lamesch, P., Xu, L., Tewari, M., Wong, S.L., Zhang, L.V., Berriz, G.F., Jacotot, L., Vaglio, P., Reboul, J., Hirozane-Kishikawa, T., Li, Q., Gabel, H.W., Elewa, A., Baumgartner, B., Rose, D.J., Yu, H., Bosak, S., Sequerra, R., Fraser, A., Mango, S.E., Saxton, W.M., Strome, S., Van Den Heuvel, S., Piano, F., Vandenhaute, J., Sardet, C., Gerstein, M., Doucette-Stamm, L., Gunsalus, K.C., Harper, J.W., Cusick, M.E., Roth, F.P., Hill, D.E., Vidal, M., 2004. A map of the interactome network of the metazoan *C. elegans*. Science 303, 540–543.

Mackinnon, A.C., Qadota, H., Norman, K.R., Moerman, D.G., Williams, B.D., 2002. *C. elegans* PAT-4/ILK functions as an adaptor protein within integrin adhesion complexes. Curr. Biol. 12, 787–797.

Moribe, H., Yochem, J., Yamada, H., Tabuse, Y., Fujimoto, T., Mekada, E., 2004. Tetraspanin protein (TSP-15) is required for epidermal integrity in *Caenorhabditis elegans*. J. Cell Sci. 117, 5209–5220.

Nievers, M.G., Schaapveld, R.Q., Sonnenberg, A., 1999. Biology and function of hemidesmosomes. Matrix Biol. 18, 5–17.

Parkinson, J., Mitreva, M., Whitton, C., Thomson, M., Daub, J., Martin, J., Schmid, R., Hall, N., Barrell, B., Waterston, R.H., McCarter, J.P., Blaxter, M.L., 2004. A transcriptomic analysis of the phylum Nematoda. Nat. Genet. 36, 1259–1267.

Pink, R., Hudson, A., Mouries, M.A., Bendig, M., 2005. Opportunities and challenges in antiparasitic drug discovery. Nat. Rev. Drug Discov. 4, 727–740.
Priess, J.R., Hirsh, D.I., 1986. *Caenorhabditis elegans* morphogenesis: the role of the cytoskeleton in elongation of the embryo. Dev. Biol. 117, 156–173.
Schnabel, R., 1995. Duels without obvious sense: counteracting inductions involved in body wall muscle development in the *Caenorhabditis elegans* embryo. Development 121, 2219–2232.
Taylor, M.J., Abdel-Wahab, N., Wu, Y., Jenkins, R.E., Bianco, A.E., 1995. *Onchocerca volvulus* larval antigen, OvB20, induces partial protection in a rodent model of onchocerciasis. Infect. Immun. 63, 4417–4422.
Tsuboi, D., Qadota, H., Kasuya, K., Amano, M., Kaibuchi, K., 2002. Isolation of the interacting molecules with GEX-3 by a novel functional screening. Biochem. Biophys. Res. Commun. 292, 697–701.
Vidal, M., 1997. In: Bartel, P.L., Fields, S. (Eds.), The two-hybrid system. Oxford University Press, New York, pp. 109–147.
Walhout, A.J., Temple, G.F., Brasch, M.A., Hartley, J.L., Lorson, M.A., van den Heuvel, S., Vidal, M., 2000. GATEWAY recombinational cloning: application to the cloning of large numbers of open reading frames or ORFeomes. Meth. Enzymol. 328, 575–592.
Walhout, A.J., Vidal, M., 2001. High-throughput yeast two-hybrid assays for large-scale protein interaction mapping. Methods 24, 297–306.
Williams, B.D., Waterston, R.H., 1994. Genes critical for muscle development and function in *Caenorhabditis elegans* identified through lethal mutations. J. Cell Biol. 124, 475–490.
Woo, W.M., Goncharov, A., Jin, Y., Chisholm, A.D., 2004. Intermediate filaments are required for *C. elegans* epidermal elongation. Dev. Biol. 267, 216–229.
Zahreddine, H., Zhang, H., Diogon, M., Nagamatsu, Y., Labouesse, M., 2010. CRT-1/calreticulin and the E3 ligase EEL-1/HUWE1 control hemidesmosome maturation in *C. elegans* development. Curr. Biol. 20, 322–327.
Zhang, H., Labouesse, M., 2010. The making of hemidesmosome structures in vivo. Dev. Dyn. 239, 1465–1476.